

LA-5743-MS  
Informal Report

UC-34  
Reporting Date: September 1974  
Issued: October 1974

C-3

GIC-14 REPORT COLLECTION  
**REPRODUCTION  
COPY**

Hydrodynamics and Burn of  
Optimally Imploded DT Spheres

by

R. J. Mason  
R. L. Morse



**los alamos**  
**scientific laboratory**  
of the University of California  
LOS ALAMOS, NEW MEXICO 87544



UNITED STATES  
ATOMIC ENERGY COMMISSION  
CONTRACT W-7405-ENG. 36

In the interest of prompt distribution, this LAMS report was not edited by the Technical Information staff.

Printed in the United States of America. Available from  
National Technical Information Service  
U.S. Department of Commerce  
5285 Port Royal Road  
Springfield, VA 22151  
Price: Printed Copy \$4.00 Microfiche \$2.25

This report was prepared as an account of work sponsored by the United States Government. Neither the United States nor the United States Atomic Energy Commission, nor any of their employees, nor any of their contractors, subcontractors, or their employees, makes any warranty, express or implied, or assumes any legal liability or responsibility for the accuracy, completeness or usefulness of any information, apparatus, product or process disclosed, or represents that its use would not infringe privately owned rights.

# HYDRODYNAMICS AND BURN OF OPTIMALLY IMPLoded DT SPHERES

by

R. J. Mason and R. L. Morse

## ABSTRACT

We review the phenomenology of optimized laser-driven DT sphere implosions leading to efficient thermonuclear burn. The optimal laser deposition profile for spheres is heuristically derived. The performance of a 7.5- $\mu\text{g}$  sphere exposed to its optimal 5.3-kJ pulse is scrutinized in detail. The timing requirements for efficient central ignition of propagating burn in the sphere are carefully explored. We discuss the difficulties stemming from hyperthermal electron production and thermal flux limitation. We give the optimal pulse parameters for spheres with masses ranging from 40 ng to 250  $\mu\text{g}$ , requiring from 50 J to 150 kJ of input energy, and the corresponding optimal performance levels. The dependence of pellet compression, heating and burn performance on the pulse energy, time scale, exponential rise rate, peak power and intensity, wavelength, and on the degree of flux limitation are all systematically described.

LOS ALAMOS NATIONAL LABORATORY



3 9338 00368 1854

## I. INTRODUCTION

High compression, as a means of enhancing the rate of energy release in systems undergoing nuclear reaction, was appreciated at Los Alamos as early as 1943.<sup>1</sup> Recently, Nuckolls et al.<sup>2</sup> at Livermore have announced a laser-driven, ablative implosion scheme for the compression of DT pellets, and Clarke et al.<sup>3</sup> at Los Alamos have summarized the results of calculations which predict that DT spheres and shells can be laser-imploded to conditions such that net break-even thermonuclear burn ensues. Also, Brueckner<sup>4</sup> at KMS Industries has discussed the implosion and burn of DT targets. The near-term prospects for laser fusion have been outlined in survey papers by Boyer,<sup>5</sup> and by Nuckolls et al.<sup>6</sup>

More recently, Fraley et al.<sup>7</sup> have described in some detail the burn physics and expansive hydrodynamics, which follow from high compression of DT. The present paper complements this burn study and expands the Ref. 3 letter with results from an extensive investigation of the laser pulse shape requirements, implosive hydrodynamics, pellet condi-

tions, and burn performance predicted for the optimized implosion of spheres.

Section II reviews the phenomenology of optimized implosions. In Sec. III we give the results of numerical studies which vary the optimal pulse parameters and pellet mass.

Conclusions are drawn in Sec. IV. Our calculations were done with the Ref. 7 computer code, modified as described in the Appendix.

## II. PHENOMENOLOGY

Under laser irradiation, electrons near the outside of the pellet, i.e., neighboring the critical surface, are heated by inverse-bremsstrahlung and various anomalous mechanisms.<sup>8</sup> In the limit of modest laser peak power this heat is transported inwards by classical (Spitzer<sup>9</sup>) thermal conductivity. With sufficiently low laser input power the thermal wave is subsonic. Heat is transferred to the ions by classical electron-ion collisions. From pressure increments in the thermal wave and from the

reaction force to the expansion of ablating ions behind it, shocks are launched toward the pellet center. The thermal wave front acts like a "leaky" piston. It abuts an ablation surface, bounding shock-compressed and shock-heated plasma. Beyond this surface the density and pressure drop, and the ions are expanding.

For an optimal implosion<sup>2,3</sup> the early power level should be kept low, so that the first shock launched is weak. Thereafter, the laser power should be time-tailored to keep the subsequent compression of the core adiabatic to a maximal degree. This is accomplished when the rising laser intensity continuously generates weak, overtaking shocks, which first coalesce to a strong shock just before the center. Upon the collapse of this final shock a high ion temperature is produced, initiating a spherical thermonuclear burn wave, which propagates out through the core of the pellet, consuming it.

#### A. Optimal Pulse

For a heuristic derivation of the optimal pulse shape consider that the pulse is driving an element of the pellet core towards the center at a speed  $v = -\frac{dR}{dt}$ . Similarly, a second lower surface is moving in at  $w = -\frac{dS}{dt}$ . The two surfaces demark a shell of mass  $\Delta m$ , width  $\Delta R = R(t) - S(t)$ , and density  $\rho = \Delta m / (4\pi R^2 \Delta R)$ . Let  $S = S_0$ ,  $R = R_0$ , and  $\Delta R = \Delta R_0$  at  $t = 0$ .

The optimal pulse brings both surfaces and all the shocks launched from the ablation surface of the core to the origin at  $t = \tau$ . The fluid in the shell moves with a speed  $u \approx v \approx w$ . The ablation surface launches weak shocks, which produce adiabatic fluid changes, so  $u \sim c$ , the speed of sound and thus  $u \sim T^{1/2}$ , the mean fluid temperature. Also,  $T \sim \rho^{\gamma-1}$ , so  $v \sim w \sim \rho^{\frac{\gamma-1}{2}}$  with  $\gamma$  the effective ratio of specific heats.

Then the assumption  $\Delta R \sim R$  leads to  $\rho \sim R^{-3}$  or  $v \sim w \sim R^{-\alpha}$ ,  $\alpha = 3(\gamma-1)/2$ . Thus, we can solve  $dR/dt = -v = c_1 R^{-\alpha}$  for the boundary condition  $R = 0$  at  $t = \tau$ , obtaining

$$R = R_0 (1 - t/\tau)^{\frac{1}{1+\alpha}}, \quad (1a)$$

so  $c_1 = R_0^{\alpha+1} / [(1+\alpha)\tau]$ . Similarly,

$S = S_0 (1 - t/\tau)^{\frac{1}{1+\alpha}}$ , so  $\Delta R = (\Delta R_0 / R_0) R \sim R$ , proving the assumption, i.e.,  $\rho = \frac{\Delta m}{4\pi R^3} (R_0 / \Delta R_0)$ . It follows that

$$v = v_0 (1 - t/\tau)^{\frac{1}{1+\alpha}}, \quad v_0 = R_0 / [(1+\alpha)\tau]. \quad (1b)$$

Finally, because work is done on the outer surface at a rate  $W = 4\pi R^2 P v$  with  $P \sim \rho T \sim R^{-3} v^2$ , i.e.,  $W \sim v^3 / R$ , and since we expect this to be proportional to the energy input rate from the laser, we conclude that the optimized laser exposure profile is

$$\dot{E}(t) = \begin{cases} E_0 (1 - t/\tau)^{-p}, & E \leq E(t_I) \\ 0, & E > E(t_I) \end{cases} \quad (1c)$$

where  $p = (3\alpha + 1) / (1 + \alpha) = (9\gamma - 7) / (3\gamma - 1) (=2$  for  $\gamma = 5/3)$ ,  $\dot{E}_0$  is some appropriate initial power, and  $E(t_I)$  is the chosen total laser input energy at shutdown time,  $t = t_I$ . This energy is given by

$$E(t_I) = \frac{\dot{E}_0 \tau}{(p-1)} (1 - t_I/\tau)^{-(p-1)}, \quad \text{assuming} \quad (2)$$

$$\Delta t_I = (\tau - t_I) / \tau \ll 1.$$

The peak power input at shutdown is

$$\begin{aligned} \dot{E}(t_I) &= \dot{E}_0 (p-1)^{\frac{p}{p-1}} \left( E(t_I) / \dot{E}_0 \tau \right)^{\frac{p}{p-1}} \\ &= (p-1)^{\frac{p}{p-1}} \left( E(t_I)^p / \dot{E}_0^p \tau^p \right)^{\frac{1}{p-1}}. \end{aligned} \quad (3)$$

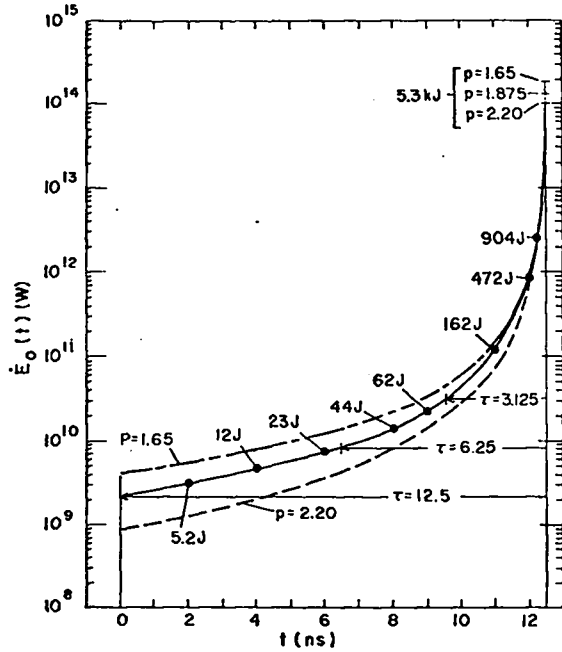


Fig. 1. Pulse shapes for the optimal implosion of a 7.5- $\mu\text{g}$  DT sphere with  $\tau = 12.5$  nsec and  $E(t_I) = 5.3$  kJ.  $\tau = 12.5$ ,  $p = 1.875$ ,  $p = 1.65$ , and  $p = 2.2$ .

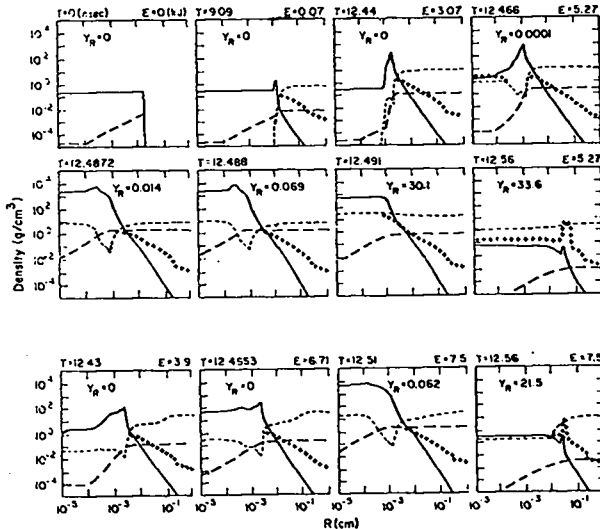


Fig. 2. Optimized implosion sequence for the 7.5- $\mu\text{g}$  sphere,  $p = 1.875$ ,  $E_0 = 2.15 \times 10^9$  W. First eight frames for  $\beta \rightarrow \infty$  and 5.3 kJ of input energy; final four frames for  $\beta = 1$  and  $E(t_I) = 7.5$  kJ — density ( $\text{g}/\text{cm}^3$ ), ---  $T_i$  (keV), +++  $T_e$  (keV), and ———  $\langle \rho R \rangle$  ( $\text{g}/\text{cm}^2$ ).

Our calculations predict that high compression can be achieved for  $p$  values ranging between 1.65 and 2.2. The corresponding effective  $\gamma$  run from 1.32 to 2.0. Figure 1 shows the pulse shapes required for the optimal implosion of 7.5- $\mu\text{g}$  DT sphere with  $\tau = 12.5$  nsec and  $E(t_I) = 5.3$  kJ. The curves are for  $p = 1.65, 1.875,$  and  $2.2$  with  $E_0$  chosen in each case to give maximum yield. Target performance details are given in Sec. III. Here it is important to note that the optimal pulse shapes are nearly identical at the end, when most of the energy is going in. In the last 500 psec, 90% of the energy is delivered and the power rises by two orders of magnitude. The  $p = 2.2$  profile has the lowest peak power -- 100 J/psec.

### B. An Optimized Implosion

Figure 2 shows the optimized implosion dynamics of a 7.5- $\mu\text{g}$  sphere. The first eight-frame sequence is for classical heat conduction, and results from the Fig. 1 pulse with  $p = 1.875$  and  $E_0 = 2.15 \times 10^9$  W. The last four frames assume a thermal speed limit on the electronic heat conduction, and required pulse retuning to  $E_0 = 2.65 \times 10^9$  W. The yield ratio (energy produced/energy invested)  $Y_R = Y/E(t_I)$  is calculated including the effects of  $\alpha$ -particle and neutron recapture during the thermonuclear burn. The dashed curves are the integral  $\int_0^R \rho dR$  of the density of solid DT, and the pellet edge is at  $R=R_e=203 \mu$ , so the full integral  $\langle \rho R \rangle \equiv \int_0^{R_e} \rho dR = 4.3 \times 10^{-3}$ . The wavelength is 10.6  $\mu$ .

By  $t = 9.09$  in the implosion sequence, electrons at the edge are at 450 eV and more than  $10^2$  times hotter than the surface ions. A first shock has been launched toward the center and there has been some shock-overtaking, so that peak density behind the shocks is 2  $\text{g}/\text{cm}^3$  for a net tenfold compression. By  $t = 12.44$  nsec the leading edge of the overtaking shock envelope is down to 10  $\mu$ , while the critical surface (where  $\rho = \rho_c = 4 \times 10^{-5} \text{ g}/\text{cm}^3$ ) has moved out to 0.12 cm. The laser shuts down at  $t = 12.466$  when the central density  $\rho(0)$  is 1.8  $\text{g}/\text{cm}^3$  and when collapse of the earliest shocks has raised  $T_i(0)$  above  $T_e(0)$  to 1.7 keV.

Burn has commenced by  $t = 12.4872$  when the yield ratio is  $Y_R = 0.014$ . At the center  $T_i(0) = 8.3$  and bootstrap-heating, chiefly from  $\alpha$ -particle

redeposition, has raised  $T_e(0)$  to 8.6 keV. The central density has been compressed to  $\rho(0) = 2.3 \times 10^3$  g/cm<sup>3</sup> and  $\langle \rho R \rangle = 2.02$ . The ion temperature exceeds 3 keV out to  $R = 1.57 \mu$ . This radius defines an initial central hot spot that includes 58 ng of DT. The hot spot is still collapsing on the origin at a mean speed of 40  $\mu$ /nsec; its mean temperature  $\langle T_h \rangle = 4.8$  keV. By  $t = 12.4880$  burn during this final implosion phase has raised  $\langle T_h \rangle$  to 8.9 keV,  $Y_R = 0.067$ , the hot spot has started to expand, and  $\langle \rho R \rangle$  is at its maximum value, 2.09.

By  $t = 12.491$  a propagating spherical burn wave has raised  $T_i$  above 8.9 keV out to  $R = 14 \mu$ , which includes 3  $\mu$ g of DT, and 90% of the yield has been released. All the yield, 177 kJ, is out by 12.56 nsec, when  $Y_R = 33.6$ , and a blast wave in the expanding plasma is heating the ions near  $R = 600 \mu$ . The final electron temperature profile is relatively flat due to the high thermal conductivity derived from the high  $T$  established by both the burn and the terminal laser desposition.

### C. Burn Conditions

High compression improves the yield from laser-heated plasmas by decreasing ratio of burn time to expansion time, and by raising the probability of  $\alpha$ -particle and neutron recapture. At high compression the best initial temperature for the fuel in the pellet core is  $\sim 7$  keV, since  $\alpha$ -particle recapture then raises  $T_i$  into the optimal 20-keV range prior to the expansion of the core, generating good yield for a minimum of energy invested. Similarly, central deposition of the energy is desirable, since then propagating burn can heat the remainder of the core. Details were given in Ref. 7; here we summarize its nomenclature and results.

For expansion times that are short compared to the characteristic burn time,  $\tau_e \ll \tau_r$ , the fractional burn-up of DT microspheres is given by

$$f_{ro} = \tau_e / 2\tau_r \quad (4)$$

with  $\tau_e = R/4C_s$ ,  $R$  the microsphere radius,  $C_s(T_i, T_e)$  the speed of sound, and  $\tau_r = \left( \frac{\rho \langle \sigma v \rangle^{-1}}{m_i} \right)^{1/2}$ , in which  $\langle \sigma v \rangle$  is Tuck's<sup>10</sup> averaged cross section and  $m_i$  is the "DT ion" mass ( $\approx 2.5$  amu).

Thus

$$\frac{\tau_e}{\tau_r} = \left( \frac{\langle \sigma v \rangle}{4C_s m_i} \right) \rho R \quad (5a)$$

and

$$f_{ro} = \left( \frac{\langle \sigma v \rangle}{8C_s m_i} \right) \rho R \quad (5b)$$

The parenthetic term in (5b) has a broad maximum ( $\approx 1/11$ ) over the range  $T_e = T_i = T = 20 \rightarrow 70$  keV, so

$$f_{ro} \approx \rho R / 11, \quad \rho R \ll 1. \quad (5c)$$

When there is considerable burnup,  $f_{ro} \gtrsim 0.1$ , depletion of the fuel slows the energy production rate, and (5c) goes over to

$$f_{ro} \approx \frac{\rho R}{6.3 + \rho R}, \quad \rho R \gtrsim 1.0. \quad (5d)$$

With full burnup 326 kJ are released per microgram of equimolar DT, so the yield from uniform microspheres is

$$Y_o / m_o = 326 f_{ro}. \quad (\text{kJ}/\mu\text{g}) \quad (5e)$$

Neutrons and  $\alpha$ -particles have mean free paths

$$\lambda_{\alpha}/R \approx \frac{1.9}{(1+122/T_e^{5/4})} / \rho R$$

$$= 0.24/\rho R \quad (\text{for } T_e = 10 \text{ keV}) \quad \text{and} \quad (6a)$$

$$\lambda_n/R = 4.6/\rho R. \quad (6b)$$

In our optimally imploded spheres, as the burn commences  $Y_R \approx 0.01 \rightarrow 0.1$ , the density is either flat at  $\rho(0)$  or gradually rising in the pellet core up to  $1.3 \rightarrow 2.0 \rho(0)$  at the ablation surface. Beyond, it, in the blow-off,  $\rho$  rapidly declines as  $\sim R^{-3}$ . Thus, for pellets it is good approximation to substitute  $\langle \rho R \rangle$  for  $\rho R$  and to use the core radius and mass for  $R$  and  $m_o$  in Eqs. (5) and (6).

For  $\langle \rho R \rangle > 0.24$  ( $T_e < 10$  keV), Eq. (6a) shows that  $\alpha$ -particles are recaptured in the core. When  $T > 4$  keV energy production from burn exceeds the pure bremsstrahlung loss. Consequently, the fuel will bootstrap heat to a higher burn temperature. At  $R = 2$  and  $T = 6$  keV, for example, Ref. 7 Fig. (10a) shows that we get a yield corresponding to  $T = 15$  keV, i.e., a tenfold improvement in the output from bootstrap-heating.

The specific internal energy of equimolar DT at degenerate densities is

$$I_o = 5.8 \times 10^{-2} \left\{ T_1 (\text{keV}) + T_{ef} (\text{keV}) \left[ 1 + \frac{\pi^2}{15} \left( \frac{T_e}{T_{ef}} \right)^2 + \dots \right] \right\} \text{ kJ}/\mu\text{g} \quad (7)$$

with  $T_{ef} = 5.7 \times 10^{-3} \rho^{2/3}$ .

The burn performance of uniform microspheres is measured by the gain factor

$$G_o \equiv \frac{Y_o}{m_o I_o} \quad (8a)$$

When there is a central hot spot from the final shock collapse in optimized implosions, the additional multiplier,  $M_c = (Y/Y_o)/(I/I_o)$ , measures the benefits of propagating burn. The  $M_c$  multiplier includes the effects of (a) decreased  $Y$  from the finite transit time of the burn wave across the core, and (b) the decreased  $I$  required when a hot spot initiates the burn. Reference 7 showed that for  $\langle \rho R \rangle > 1.0$ ,  $G_o(T = 6 \text{ keV}) > G_o(T = 20 \text{ keV})$  for at least a 3.3-fold decrease in the input energy requirements to a uniform microsphere. Also, it gave the rule of thumb that  $M_c > 1$  for  $\rho R > 2$ .

The Ref. 7  $G_o$  and  $M_c$  predictions for DT microspheres neglected the effects of neutron recapture. From (6b) we see that recapture should enhance bootstrap-heating and propagation for  $\langle \rho R \rangle \geq 4$ . Consequently, we introduce the multiplier,

$$M_n \equiv G_o^n / G_o, \quad (8b)$$

to measure the yield increase  $Y_o \rightarrow Y_o^n$ , from neutron redeposition in uniformly heated microspheres and we define

$$M_c^n \equiv \left( Y^n / Y_o^n \right) / \left( I / I_o \right) \quad (8c)$$

as the central ignition multiplier, when both  $\alpha$ -particle and neutron recapture are significant.

Laser energy  $E(t_I)$  couples through the implosion process to the core of a pellet with an efficiency,

$$\epsilon \equiv m_o I_c / E(t_I) \quad (8d)$$

in which the core energy  $m_o I_c$  is partly established by burn-preheat during the core compression to maximum  $\langle \rho R \rangle$ . Also, the internal energy of the core of a pellet may differ from that of its corresponding microsphere (having the same  $\langle \rho R \rangle$  and mean  $T$  values), because of the density dependence of internal energy that comes with degeneracy. A final multiplier

$$M_I = I / I_c \quad (8e)$$

corrects this discrepancy.

Thus, our measure of overall pellet performance becomes

$$Y_R = \frac{Y}{E(t_I)} = \frac{\epsilon Y}{m_o I_c} = \epsilon G_o M_c^n M_I. \quad (9)$$

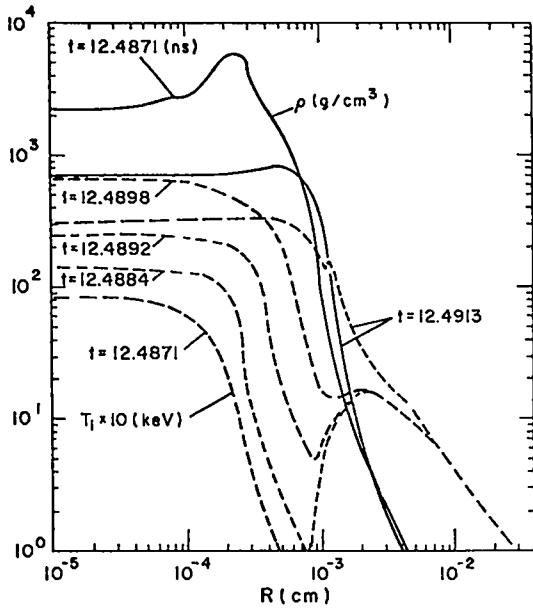


Fig. 3(a). Propagating burn in the 7.5- $\mu$ g sphere following ignition. — density --- temperature.

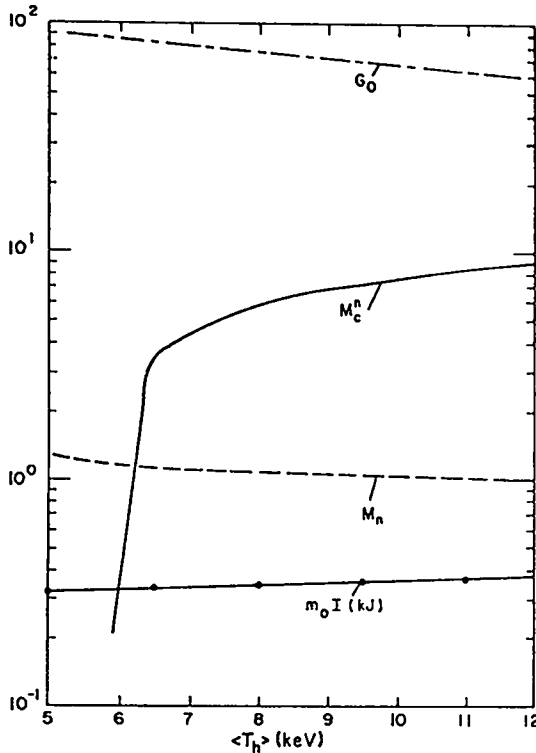


Fig. 3(b). Temperature dependence of the burn performance multipliers.

In the Fig. 2 implosion the maximum  $\langle \rho R \rangle$  is 2.09 at  $t = 12.4880$ . Since bootstrap-heating subsequently raises the core above 20 keV, a burnup fraction,  $f_{ro} = 0.25$ , is implied by (5d). The total yield of 177 kJ then tells us through (5e) that the active core mass with uniform initial heating would be 2.17  $\mu$ g. However, the Fig. 2 burn starts from a central hot spot, and Ref. 7 showed that under optimal conditions only 70-75% of the uniform yield is extracted via propagating burn, so we take  $m_o = 2.17/0.75 = 2.89 \mu$ g. This constitutes 39% of the total pellet mass. At peak  $\langle \rho R \rangle$  we calculate  $m_o I_c = 310$  J, so  $\epsilon = m_o I_c / E(t_I) = 0.059$ . This includes 100 J of recaptured energy generated during the last picosecond of implosion. The inner 58 ng ( $=m_h$ ) of the core is at an average temperature  $\langle T_h \rangle = 8.9$  keV. The remainder of the core is at an average temperature  $T_c = 0.49$  keV. Figure 3(a) details the progress of the spherical burn wave that ignites the cold region in 3 psec, crossing it at a speed of  $\sim 4 \times 10^8$  cm/sec. The temperature dependence of our various multipliers is plotted in Fig. 3(b). Its results represent an extension of the Ref. 7 burn study to the present special case, where  $m_o = 2.89 \mu$ g,  $T_c = 0.49$ ,  $\langle \rho R \rangle = 2.09$ , and  $f_h = m_h / m_o = 0.02$ . Figure 3(b) shows that at  $\langle T_h \rangle = 8.9$ ,  $G_o = 72$ ,  $M_c^n = 6.8$ ,  $M_n = 1.03$ , and since  $m_o I = 0.35$  kJ,  $M_I = 1.13$ . Thus, the burn study results for the Fig. 2 implosion parameters predict a yield ratio

$$Y_R = \epsilon G_o M_c^n M_n M_I = (0.059) 72 (6.8) 1.03 (1.13) = 33.6,$$

indicating the origins of the ratio computed in the full implosion calculation.

Figure 3(b) makes an important addition to the earlier burn study, by showing that although  $G_o$  ( $\rho R = 2$ ) improves as  $T = 10 \rightarrow 3$  central ignition essentially fails for  $T < 6.5$  keV.

Also, it should be noted that when the neutron redeposition is ignored, so that the neutrons are allowed to freely escape from the pellet, then the optimal yield ratio drops to  $Y_R = 25.8$ . Correspondingly,  $M_n = 1.0$  and  $M_c^n \rightarrow M_c = 4.8$ .



#### D. Compression and Shock Heating

Compression of the core should be carried out as adiabatically as possible to keep the energy demands on the laser to a minimum. This means that the internal energy will at times be near its degeneracy floor. For  $T_e \rightarrow T_i \rightarrow 0$ , (7) shows that  $I \rightarrow 3.3 \times 10^{-4} \rho^{2/3}$  kJ/ $\mu\text{g}$ , which is 69 J/ $\mu\text{g}$  at  $\rho = 3 \times 10^3$  g/cm<sup>3</sup>, or the thermal equivalent of 0.59 keV at classical densities. Clearly, this influences the energy requirements of the cold outer region of the Fig. 2 core, prior to its heating by propagating burn. Another energy sink is the  $\sim 0.6$  J/ $\mu\text{g}$  needed for full ionization of the DT by the early shocks in the implosion sequence. These degeneracy and ionization energy effects are fully included in the equation-of-state tables accessed in our calculations. Degeneracy should also affect thermal transport to the core. Still, classical Spitzer transport coefficients are used here. As pointed out by Brysk et al.,<sup>11</sup> the proper forms for the degenerate coefficients for laser fusion conditions remain somewhat uncertain. From the use of approximate, interpolated degenerate coefficients Brysk reports only minor changes in the timing requirements for optimal implosions.

The first shock in our calculations is usually strong (its Mach number  $M \gg 1$ ) with the DT started at  $10^{-7}$  keV (1°K). If we take the 2.5-fold compression point (where  $\rho = 0.54$  g/cm<sup>3</sup>) to be the location of the first shock, then in the Fig. 2 optimized implosion, for example, we find the shock to be at  $R_0 = 1.95 \times 10^{-2}$  cm, when  $t = 0.3$  nsec, and moving at  $v_0 = R_0/2\tau = 7.8 \times 10^5$  cm/sec, in agreement with (1b) for  $\alpha=1$ . Also the  $R(t)$  and  $v(t)$  values for this point follow (1a,b) to within 10%, for at least the first 10 nsec. Convergence increases the shock speed, so that by  $t = 9$ ,  $v = 1.3 \times 10^6$  cm/sec. At  $t = 12.455$ , just before the collapse of the first shock at the origin,  $v = 2.4 \times 10^7$  cm/sec.

Although the first shock is strong, the temperature established by its central collapse is regulated by  $v_0$  and ultimately  $\dot{E}_0$ . One wants  $v_0$  to be great enough to avoid premature shock-overtaking outside the origin by the stronger shocks which follow. But also,  $v_0$  should be kept low to minimize the heating from the central collapse of the first shock itself, which would limit the compression

achieved from the follow-on shocks. Both criteria can be satisfied, if  $\tau$  is large enough. Our simulations show that  $\tau > 10$  nsec suffices for pellet masses in the range  $40 \text{ ng} < m < 250 \mu\text{g}$ .

One interpretation is that in the optimal scheme each shock falling on the origin cushions the one after it. As the central density  $\rho(0)$  rises, strong shocks driven by a given pressure  $P$  fall on the origin with a decreased speed,  $v = (4P/3\rho(0))^{1/2}$ , relative to the speed of the same shocks without precompression. With decreased  $v$  the final shock Mach number and central heating are reduced, leading to a higher  $\langle \rho R \rangle$ . Judicious timing preserves just enough of the heating for an optimal initiation of propagating burn.

Figure 4(a) displays the major pellet properties in the Fig. 2 implosion at the instant of laser shutdown,  $t = 12.466$ . Near the origin  $T_i > T_e$ , from the collapse of the earliest shocks. In the region beyond  $13 \mu$  the pressure drops rigorously as  $R^{-3}$ . Outside  $R = 10^2 \mu$  the density acquires this same dependence,  $\rho \sim R^{-3}$ , while the  $T_e$  profile becomes flat, and  $T_i \sim R^{-2}$ . The rapid  $T_e$  decline near  $R = 13 \mu$  marks the location of the ablation surface. The flow velocity reversal, and the  $P$  and  $\rho$  drop off beyond this surface also identify it as a deflagration front.<sup>12-14</sup> The fluid just ahead of the front is moving at  $u = 2.9 \times 10^7$  cm/sec, and the front itself is falling on the origin at  $u_D = 3.2 \times 10^7$  cm/sec, measured from the trajectory of the density peak. Thus, the front is penetrating the mass ahead at  $u_p = u_D - u = 3.0 \times 10^6$  cm/sec. The small speed ratio,  $u_p/u_D = 0.094$ , is consistent with the sharp density drop across the front. But, since the maximum sound speed is  $C_s = 6.6 \times 10^6$  cm/sec (at  $R = 12 \mu$ ), we conclude that the Chapman-Jouguet condition,  $u_D = u + C_s$ , is not strictly obeyed. This is not surprising, in view of the highly convergent and time-dependent nature of the problem at  $t \rightarrow \tau$ . The peak density rises from 400 to 680 g/cm<sup>3</sup> in just the 5 psec preceding shutdown.

The insert in 4(a) shows the effects of pulse detuning on the density profile at laser shutdown. The solid curve repeats the main figure's profile, which is for the optimal initial power,  $\dot{E}$  ( $= 2.15 \times 10^9$  W). With  $\dot{E} = 3.0 \times 10^9$  W the first shock has already hit the origin, raising the density prematurely. We shall see below that this provides

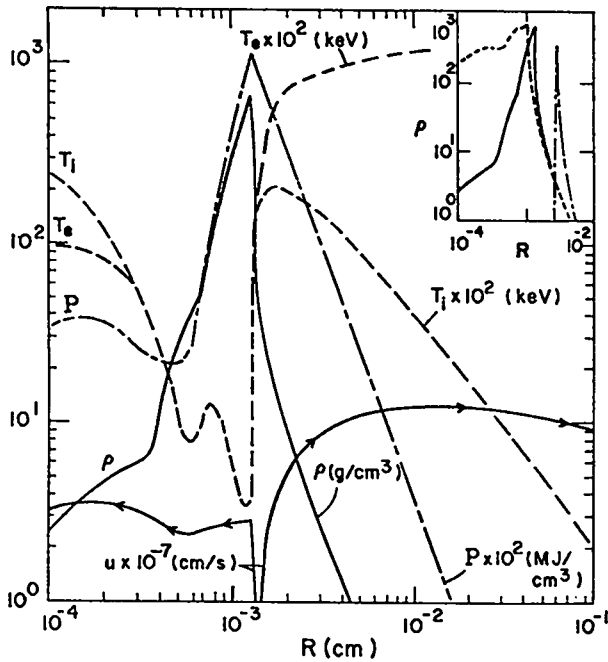


Fig. 4(a). Conditions in the 7.5- $\mu$ g sphere at the moment of laser shutdown,  $t_s = 12.466$ . ---  $T_i \times 10^2$  (keV), —  $T_e$  (keV),  $P \times 10^{-2}$  (MJ/cm $^3$ ), —  $\rho$  (g/cm $^3$ ),  $\leftrightarrow$   $u \times 10^{-7}$  (cm/sec). Insert shows the density profiles at shutdown when  $E_0 = 2.15 \times 10^9$  W (which is the optimal tuning corresponding to the main figure), and detuned to  $E_0 = 1.5 \times 10^9$  W (—), and to  $E_0 = 3.0 \times 10^9$  W (---).

too much of a cushion for the later shocks, so that 1.4 keV is the highest central temperature achieved, and ignition fails. With  $E_0$  reduced to  $1.5 \times 10^9$  W the profile manifests premature shock-overtaking, which results in a 20-keV collapse temperature and inefficient propagating burn.

In Sec. A we discussed the implosion of a mass layer within a pellet to motivate our choice for the optimal pulse. Figure 4(b) tracks the evolution of one such layer in our Fig. 2 implosion. The layer was chosen to be inside the ablation front and at the mean density at the commencement of burn. Initially, its position is  $R_0 = 90 \mu$  and its width  $\Delta R_0 = 0.61 \mu$ . We have marked the total energy deposited by the time the layer has reached its specified R. The layers  $\rho$ , and T and u values, and the pellets  $\langle \rho R \rangle$  are plotted versus R(t).

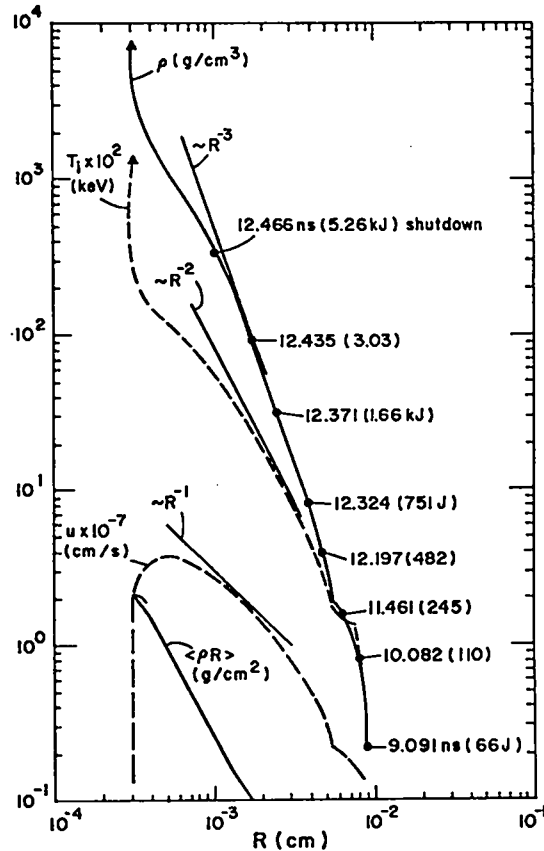


Fig. 4(b). The evolution of conditions in a mass layer, initially at  $R_0 = 90 \mu$ , in the 7.5- $\mu$ g sphere, as its optimized implosion proceeds, —  $\rho$  (g/cm $^3$ ), ---  $T_i \times 10^2$  (keV), —  $u \times 10^{-7}$  cm/sec, and —  $\langle \rho R \rangle$  (g/cm $^2$ ).

There is no motion of the layer until the first shock strikes it at  $t = 9$  nsec. There follows a strong shock compression producing  $\rho \approx 0.84$  g/cm $^3$  by  $t = 10$  nsec. Then, as the energy deposition runs from 300 J to 3 kJ, we see that  $\rho \sim R^{-3}$ ,  $T \sim R^{-2}$ , and  $u \sim R^{-1}$ , as predicted in Sec. A for  $p = 2$  ( $\alpha=1$ )—even though  $p = 1.875$  is, in fact, used here. Central shock heating and burn retard the compression for  $R < 5 \mu$ . The kinetic energy of the shell starts to go over to thermal energy, and then burn takes the temperature up beyond 15 keV. Expansion of the central pellet hot spot, as propagating burn begins, then pushes the shell density over  $7 \times 10^3$  g/cm $^3$ . Note that at laser shutdown  $\langle \rho R \rangle$  is already large enough ( $\sim 0.25$ ) for  $\alpha$ -particle recapture in the pellet.

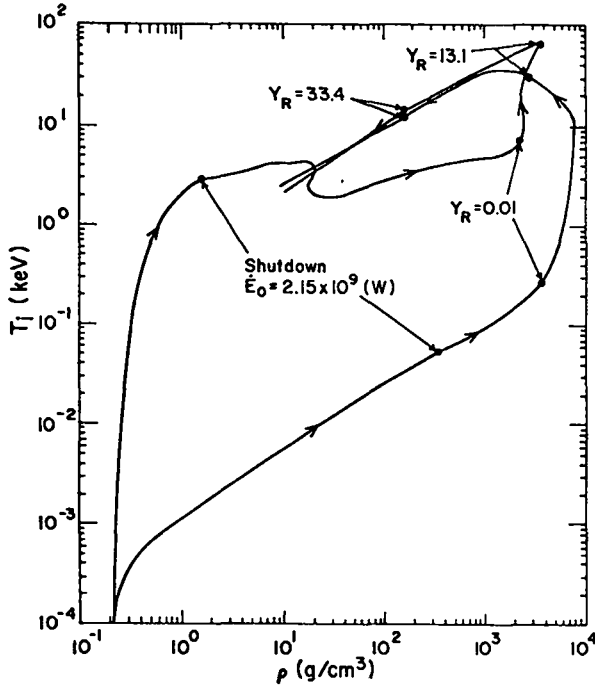


Fig. 4(c). The  $T_1, \rho$  adiabats for the optimized Fig. 2 implosion. Trajectories are given for the layer discussed in (b) and for the central calculation zone.  $\dot{E}_0 = 2.15 \times 10^9 \text{ W}$

Finally, we return to the question of pulse tuning. Figure 4(c) shows the significant  $T_1, \rho$  adiabats for the optimized Fig. 2 implosion. The lower curve shows the evolution of the Fig. 4(b) mass layer. The upper curve tracks the conditions in the central zone of the pellet. The mass layer is shock compressed to  $\sim 0.84 \text{ g/cm}^3$ , and 1 eV and then follows a  $T \sim \rho^{2/3}$  adiabat until  $\rho > 2 \times 10^3 \text{ g/cm}^3$ . The central zone sees a stronger convergent shock that compresses it  $\sim$  thirtyfold to  $6 \text{ g/cm}^3$  and onto a temperature plateau near 4 keV. When the yield starts to come out,  $Y_R = 0.01$ , the layer is highly degenerate at  $\rho = 3.6 \times 10^3$  and only 0.25 keV. During the burn it is heated to over 35 keV. Most of the yield is out by the time the layer and center have expanded down to  $\rho = 150 \text{ g/cm}^3$ . Following laser shutdown and arrival of the first shock at the center, there is some, slight conductive cooling of the center down to 2 keV. Then, as the remaining shocks coalesce at the origin, there is adiabatic compression of the central zone to  $\rho = 2 \times 10^3 \text{ g/cm}^3$

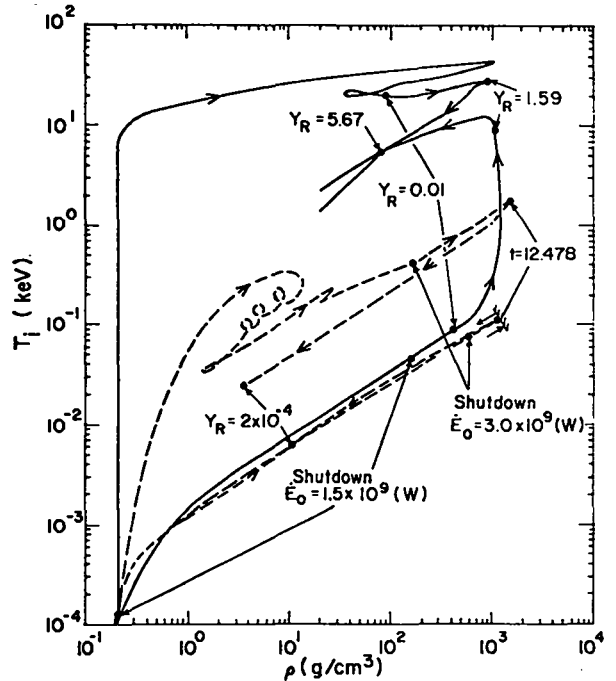


Fig. 4(d). The adiabats for  $\dot{E}_0 \times 3.0 \times 10^9 \text{ W}$  ----, and for  $\dot{E}_0 = 1.5 \times 10^9 \text{ W}$  ———, corresponding to the detuned cases in the 4(a) insert.

and 5 keV. Burn during the final implosion phase raises the zone to 7.5 keV ( $Y_R = 0.01$ ), and then bootstrap-heating takes it up to 65 keV. This complex behavior is concomitant with optimal yield from the 7.5- $\mu\text{g}$  pellet.

Figure 4(d) shows the response to mistuned pulses. When  $\dot{E}_0 = 3 \times 10^9 \text{ W}$  the central zone shock heats to only 0.3 keV. The first shock is premature so there follows a subsequent expansion down to 30 eV. All this occurs well before laser shutdown—unlike the tuned case where the arrival and shutdown are nearly simultaneous. Following shutdown the  $\dot{E}_0 = 3 \times 10^9 \text{ W}$  pulse brings both the layer and the center up to  $1.5 \times 10^3 \text{ g/cm}^3$ . But, since the center goes only to 1.8 keV, there is no ignition and negligible yield. On the other hand, with  $\dot{E}_0$  too low at  $1.5 \times 10^9 \text{ W}$ , the first shock takes the center directly to 15 keV at  $\rho = 0.84 \text{ g/cm}^3$ . The subsequent compression is nearly isothermal, due to the good thermal conduction above 15 keV. When  $Y_R = 0.01$  the center is at 20 keV, and still compressing. The high central temperature limits the

maximum density achieved to  $1.2 \times 10^3$  g/cm<sup>3</sup> in both the layer and the center, and because of the lower  $\langle \rho R \rangle$  achieved ( $\approx 1.20$  here, as compared to 2.09 with the optimal pulse), there is only time to raise the layer to 12 keV prior to expansion. This limits  $Y_R$  to 5.64.

#### E. Thermal Transport and Flux Limitation

Electron thermal conduction transfers the laser energy from the critical surface to the ablation front. The electrons are highly collisionless near the critical surface. Reference 15 carried out simulations of the collisionless conductivity, and showed that where the total electron density is  $n$ , the minimum peak hot electron velocity  $v_h$  needed to transport an energy flux  $q$  (W/cm<sup>2</sup>) is given by

$$\left. \frac{q}{2\pi m_e v_h^3} \right|_{\max} = 1/16. \quad (10a)$$

This assumes planar, one-dimensional geometry, steady transport, and that the minimum  $v_h$  occurs with nearly flat hot and cold distribution functions, such that  $v_h = (3kT_h/me)^{1/2}$ , and  $T_h = 2T_e$  relates the temperature of the hot electrons to the mean temperature. When (10a) is expressed in terms and adjusted to include energy flow in three dimensions, it becomes

$$q|_{\max} = \beta \frac{\bar{c}}{4} \left( \frac{3kT_e}{2} \right) \quad (10b)$$

with  $\bar{c} = \left( \frac{\beta}{\pi} \frac{kT_e}{m_e} \right)^{1/2}$  and  $\beta \approx 1.0$ . This agrees with the work of Forslund<sup>16</sup>, and the limiter employed in the Livermore Lasnex<sup>2,6</sup> simulation code. If the laser-generated distribution is stable but off-optimum, (10b) tells us that  $T_h$  is above the minimum and  $\beta < 1$ . Alternatively, the distribution could be unstable,<sup>17</sup> with a long growth time from, say, the presence of a very weak hot electron stream, i.e.,  $n_h/n \ll 1$ , then  $\beta > 1$ .

At the critical surface under limitation the peak laser power obeys  $q(t_I) \sim n_c T_c^{3/2}$  from (10b). Consider a series of optimal implosions at different wavelengths  $\lambda$ . The peak intensity goes as  $q(t_I) \sim \dot{E}(t_I)/R_c^2$ . In the blowoff  $n \sim R^{-3}$ , the critical density obeys  $n_c \sim \lambda^{-2}$ , and simulations can provide  $r$  in the phenomenological rule  $\dot{E}(t_I, \lambda) \sim \lambda^r$ . Thus, the coronal temperature will scale as

$$T_c \sim (q/n_c)^{2/3} \sim \left[ \frac{\dot{E}(t_I, \lambda)}{n_c R_c^2} \right]^{2/3} \quad (11a)$$

$$\sim \lambda^{2/3(2/3 + r)}$$

We shall see in Sec. III that, typically,  $r \approx -0.2$ , so  $T_c \sim \lambda^{0.3}$ . This gives a 2.0-fold increase in temperature from the change  $\lambda = 1.06 \rightarrow 10.6 \mu$ . Similarly, as we go to different pellet masses at fixed  $\lambda$ ,  $R_c \sim m^{1/3}$ , and thus

$$T_c \sim q^{2/3} \sim \left( \frac{\dot{E}(t_I, m)}{R_c^2} \right)^{2/3} \quad (11b)$$

$$\sim m^{2/3(s - 2/3)},$$

in which  $\dot{E}(t_I, m) \sim m^s$  can be derived from implosion calculations. In fact, we find that  $s = 0.36$ , so  $T_c \sim m^{-0.20}$ , giving a twofold decrease in coronal temperature as we go from, say,  $m = 7.5 \rightarrow 250 \mu\text{g}$ .

At low-energy flux levels classical thermal conductivity is accurate. To bring in limitation smoothly at high levels, we make the substitution

$$\left( k_e \frac{\partial T_e}{\partial r} \right)^{-1} + \left( k_e \frac{\partial T_e}{\partial r} \right)^{-1} + \quad (12)$$

$$\left[ \frac{\beta n_c}{4} \left( \frac{3}{2} kT_e \right) \right]^{-1}$$

in our simulation code [Eq. (b-2b) in Ref. 7].

The last four frames in Fig. 2 show details of the optimized implosion of the 7.5- $\mu$ g pellet for  $\beta = 1$ . To maintain the optimal yield it has been necessary to retune the pulse to  $\dot{E}_0 = 2.65 \times 10^9$  W, and to raise the input energy to 7.5 kJ. Thus limitation decreases the optimal yield ratio  $Y_R^*$  to 23.6. Also, the coronal temperature at the critical surface rises from 12.3 keV with  $\beta \rightarrow \infty$  to 48 keV when  $\beta = 1$ . The  $T_e$  profile manifests a plateau near the critical surface, but otherwise the implosion phenomenology is the same as for  $\beta \rightarrow \infty$ . The greater energy input supports the higher coronal temperature. The increase in  $\dot{E}_0$  maintains proper timing of the intermediate shocks, which tend to be delayed as limitation slows the rate of rate energy transport from the critical surface to the ablation front.

Use of the limiter can provide a first estimate of the effects of hyperthermal electron transport. Generally, the results which follow show little difference between  $\beta = 1$  and  $\beta \rightarrow \infty$  calculations for  $\lambda = 10.6 \mu$ , and this is encouraging. On the other hand, flux-limited diffusion fails to model core preheat<sup>18</sup> from any hyperthermal electrons generated in the corona, and misses geometric<sup>19</sup> effects associated with the angular momentum of electrons, rattling about in the corona and possibly missing the core. Furthermore, the effects of plasma instabilities, from ion and magnetic field fluctuations and from the time dependence of the laser deposition itself, may lie outside the scope of any diffusive transport treatment. For an accurate description of these effects, a fully self-consistent, kinetic transport model will be required. In the interim, problems associated with hot electrons can be reduced by going to shorter wavelengths and/or to larger pellets, taking advantage of the Eq. (11) scaling rules for the coronal temperature.

### III. PARAMETER STUDY RESULTS

#### A. $\dot{E}_0$ , $E(t_I)$ , and $\dot{E}(t_I)$ Dependence

Figure 5(a) has been constructed from the results of many runs to show how target response changes as  $\dot{E}_0$  and  $E(t_I)$  in the optimal pulse (1c) are varied. The results are for the 7.5- $\mu$ g sphere exposed to 2.5, 5.3, and 12 kJ of CO<sub>2</sub> light with  $p = 1.875$ ,  $\tau = 12.5$ , and  $\beta \rightarrow \infty$ . The figure collects much data, but it is instructive to show it together. First, we give the yield ratios observed for 12-

and 5.3-kJ input cases--the yield with 2.5 kJ is negligible. Then we show the maximum central densities  $\rho(0)$  achieved with the three input energies, and plot  $\langle \rho R \rangle$  for the 5.3-kJ case--it obviously tracks  $\rho(0)$ . Finally, we include the central ion temperatures  $T(0)$ ; they prove to be an extremely useful diagnostic in "tuning up" the pulse. For 12 and 5.3 kJ we give the  $T(0)$  registered at the time when 53 J has been released (this corresponds to  $Y_R = 0.01$  at the 5.3-kJ energy--which we find to be optimal). When  $\dot{E}_0$  exceeds  $2.2 \times 10^9$  W the burn effectively ceases, so here we give maximum  $T(0)$  achieved in the implosions. Similarly, we give the maximum  $T(0)$  registered in each of the 2.5-kJ implosions.

With 5.3 kJ of input,  $T(0)$  runs from 20 keV at  $\dot{E}_0 = 1.5 \times 10^9$  W to 1.2 keV at  $3 \times 10^9$  W. The central temperature is 6.6 keV at the  $\dot{E}_0$  of maximum yield. The yield ratio rises slowly to its 33.6 maximum at 6.6 keV and then drops precipitiously. Observe that  $\rho(0)$  and  $\langle \rho R \rangle$  have their maxima near the optimal yield point. Pellet response to the optimal tuning has been carefully scrutinized in Sec. II, B-D. Figure 3(b) shows the sharp decline in the effectiveness of propagating burn below 6.6 keV. We conclude that the optimal tuning makes maximal use of propagating burn.

When 12 kJ is supplied we get the same  $T(0)$  dependence except below 6.5 keV where the yield is negligible. Generally, the  $\rho(0)$  values are higher than in the 5.3-kJ runs. At the density maximum  $T(0)$  is 16 keV. There is some increase in the absolute yield produced, but the input energy is so much larger that  $Y_R$  drops. Alternatively, with 2.5 kJ supplied  $T(0)$  is always below 3 keV for  $\langle \rho R \rangle$  above 0.65. The  $\langle \rho R \rangle$  at maximum density is only 0.88, while  $T(0)$  there is 1.2 keV. There is no ignition and negligible yield.

In general, when the input energy is increased,  $T(0)$  increases at the  $\dot{E}_0$  point giving maximum  $\langle \rho R \rangle$ . More refined calculations place the optimum  $E(t_I)$  at 5.3 kJ  $\pm 10\%$ . We conclude that for the overall optimum tuning one must provide just enough energy to put the maximum  $\langle \rho R \rangle$  just above the 6.5-keV knee in the central ignition curve,  $M_c(T)$  of Fig. 3(b).

Thus, in optimized implosions  $\dot{E}_0$  controls the central temperature achieved, and compression is linked to the energy supplied. The energy is

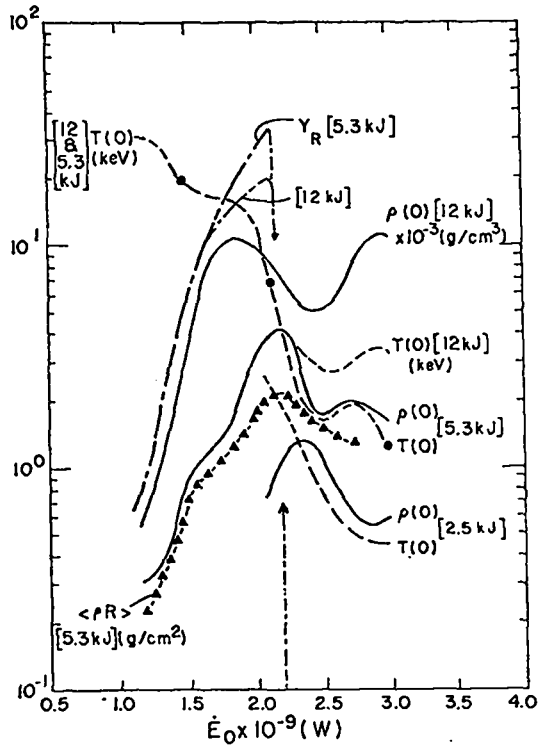


Fig. 5(a). Pellet conditions in the 7.5- $\mu$ g sphere for different  $\dot{E}_0$  and  $E(t_I)$  choices  
 $\frac{Y_R}{\rho(0)}$   
 $T(0)$  (keV), —  $\rho(0)$  ( $g/cm^3$ ), and  $\blacktriangle\blacktriangle\blacktriangle$   $\langle\rho R\rangle$  ( $g/cm^2$ ).

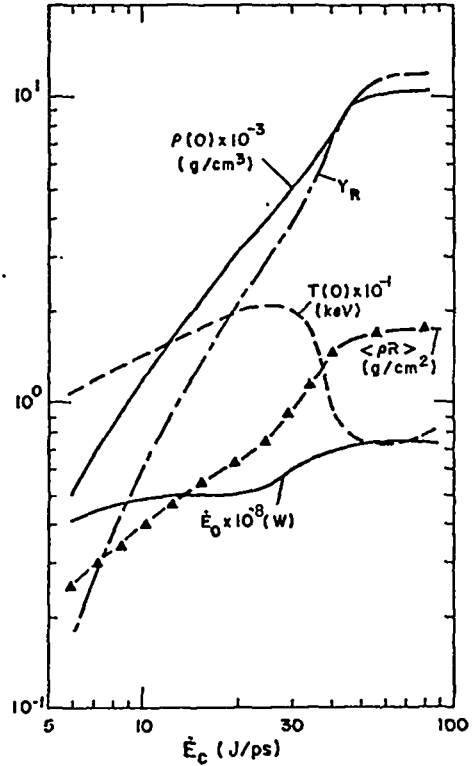


Fig. 5(b). Response of conditions in a 0.7- $\mu$ g sphere to a peak power ceiling,  $\dot{E}_c$  on the optimized pulse.

however, directly related to the peak power in optimal pulses [see (2)], so it is not immediately clear whether  $E(t_I)$  or  $\dot{E}(t_I)$  is important to compression. Figure 5(b) demonstrates that peak power is the controlling parameter. It shows the performance of a 0.7- $\mu$ g sphere under 700 J of  $CO_2$  light ( $\beta \rightarrow \infty$ ) with the energy deposited in accordance with (1c) (again  $\tau = 12.5$  nsec, and  $p = 1.875$ ) until a ceiling rate  $\dot{E}_c$  was reached. Thereafter, energy was supplied at the  $\dot{E}_c$  rate until the full 700 J were delivered. The figure plots the optimized pellet conditions vs  $\dot{E}_c$ . With no ceiling imposed the peak power just prior to laser shutdown is 85 J/psec ( $8.5 \times 10^{13}$  W);  $Y_R = 13.2$  and  $\dot{E}_0 = 7 \times 10^7$  W. The yield is off slightly at 45 J/ps, and drops rapidly with further reductions in the ceiling. For break-even  $\dot{E}_c > 12$  J/psec is required. Going from 45 J/psec to 25 J/psec the optimal retuning in  $\dot{E}_0$  compensates for the lost  $\langle\rho R\rangle$  by raising the peak central temp-

erature to 21 keV [which gives the best fractional burnup (4) in the absence of bootstrap-heating]. With still lower  $\dot{E}_c$  these higher  $T(0)$  become inaccessible. With the ceiling imposed, no improvement in performance derives from increases in  $E(t_I)$ . This is not really surprising, in view of the arguments preceding (1), which suggest that the density achieved to a given time is proportional to the instantaneous power.

#### B. The Time Scale $\tau$

The results, thus far, have all been for the fixed time scale  $\tau = 12.5$  nsec. Figure 6 shows how the optimal performance changes with  $\tau$ . Again, we are considering the 7.5- $\mu$ g sphere with  $p = 1.875$ ,  $\lambda = 10.6 \mu$ , ( $\beta \rightarrow \infty$ ), and  $E(t_I) = 5.3$  kJ. For each  $\tau$  considered  $\dot{E}_0$  was tuned to determine the maximum  $Y_R$ . This is plotted along with the corresponding pellet conditions.

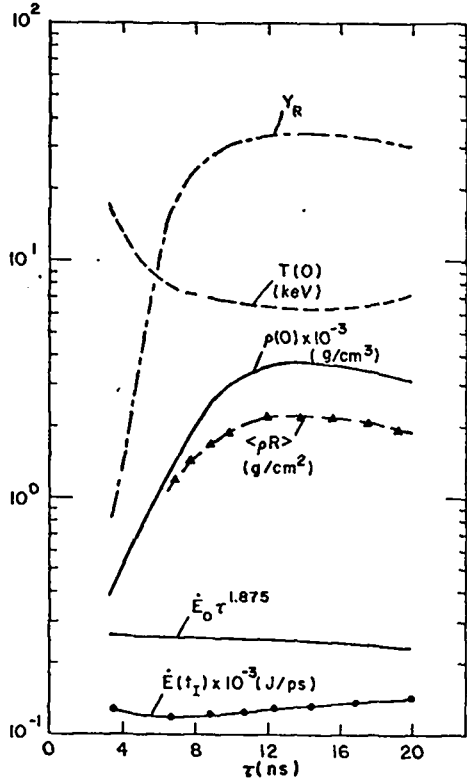


Fig. 6. Optimal performance characteristics for the 7.5- $\mu\text{g}$  sphere vs  $\tau$ .

The yield ratio has a broad maximum near 15 nsec. It drops rapidly as we go below 8 nsec, and slowly as  $\tau$  approaches 20 nsec. Over this range of  $\tau$  values, the product  $\dot{E}_0 \tau^p$  is very nearly constant. This is significant because it tells us that all the optimized profiles for different  $\tau$  are, in fact, the same curve with different extensions to early time.

To see this connection, consider the following. Suppose we have found the optimal pulse for a given  $\tau$  value, and we choose to deposit laser energy in accordance with this profile, but starting at a new time  $t_1 < \tau$ . Then the new deposition rule is

$$\begin{aligned}
 E(t) &= \dot{E}_0 \left(1 - \frac{t + t_1}{\tau}\right)^{-p} \\
 &= \frac{\dot{E}_0 \tau^p}{(\tau - t_1)^p} \left(1 - \frac{t}{\tau - t_1}\right)^{-p}
 \end{aligned}
 \tag{13a}$$

$$= \dot{E}'_0 (1 - t/\tau')^{-p}
 \tag{13b}$$

with  $\tau' = \tau - t_1$  and  $\dot{E}'_0 = \dot{E}_0 (\tau/\tau')^p$ . The new starting point lies on an extension of the old pulse, if the scaling rule

$$\dot{E}_0 \tau^p \sim \text{const}
 \tag{13c}$$

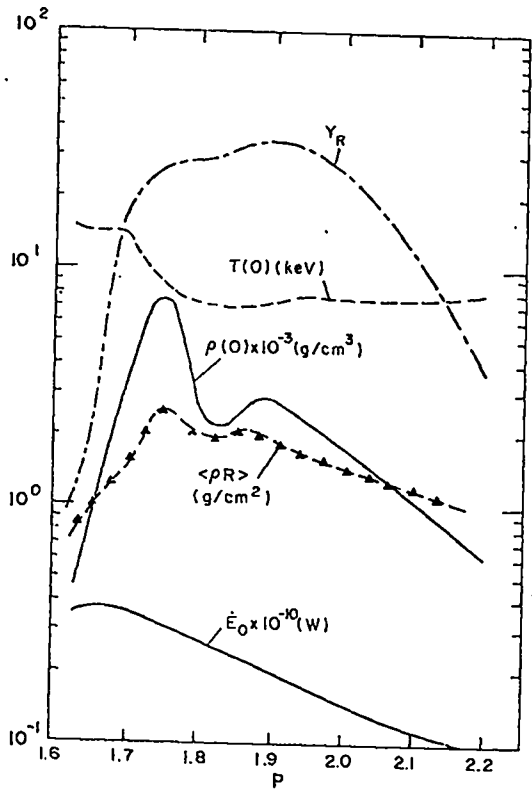
is observed. The Fig. 6 results obey this rule, so they all lie on the single optimal profile for 7.5  $\mu\text{g}$ ,  $p = 1.875$ .

Only 23 J is deposited during the first 6 nsec of the Fig. 1  $p = 1.875$  profile. One might choose to start the deposition at  $t_1 = 6$  nsec to ease the laser timing requirements. Figure 6 shows, however, that the early deposition is quite important, since  $Y_R$  drops from 33.6 to 13, if  $\tau$  is reduced to  $\tau = 6.5$  nsec. The early part of the pulse is needed to launch weak shocks to cushion the final shock collapse. If  $\tau$  is too short, here  $< 8$  nsec, the early shocks are themselves too strong, generating excessive preheat. Also, for  $\tau < 5$  nsec  $\dot{E}_0$  must be so intense to launch converging shocks that the thermal front tends to burn through the ablation surface it supports. Thus, with  $\tau = 3.1$  in Fig. 6,  $T(0)$  climbs to 18 keV. The improvement in  $\rho(0)$  and  $\langle \rho R \rangle$  as we go toward 12 nsec follows from a reduction of this preheat. On the other hand, the fall-off in performance as  $\tau \rightarrow 20$  nsec occurs because enough time is available for the earliest shocks to reflect and recede somewhat from the origin prior to the arrival of the main, collapsing shock envelope.

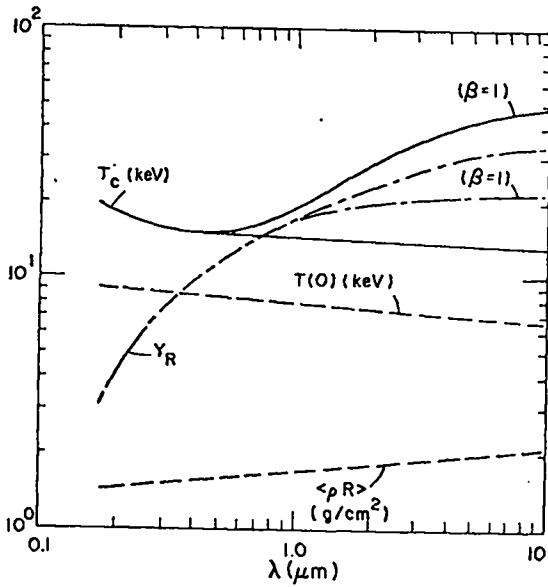
### C. $p$ , $\lambda$ and $\beta$ Dependence

Figure 7(a) determines bounds for our choice of the exponent  $p$ . Again, the results are for the 7.5- $\mu\text{g}$  pellet under the usual conditions. The best  $Y_R$  is at  $p = 1.9$ . The dropoff is less than 10% over the range  $1.85 < p < 1.95$ , and less than 30% for  $1.68 < p < 2.1$ . There is a rapid decline in  $Y_R$  for  $p < 1.68$ , and a more gradual decline for

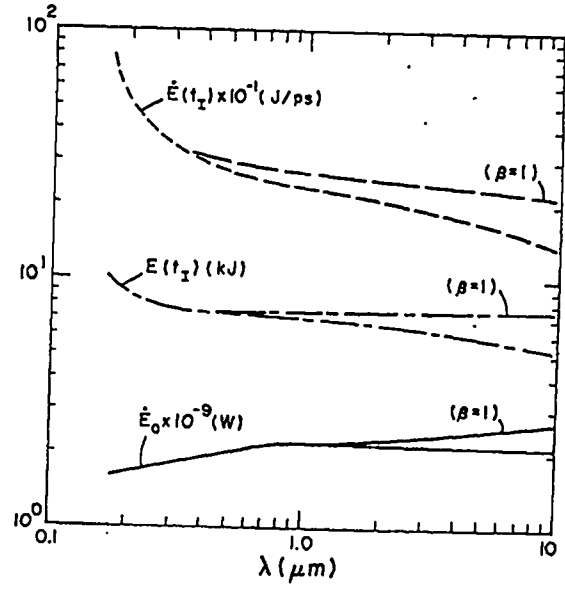
Fig. 7. Dependence of the optimized performance and pulse parameters on



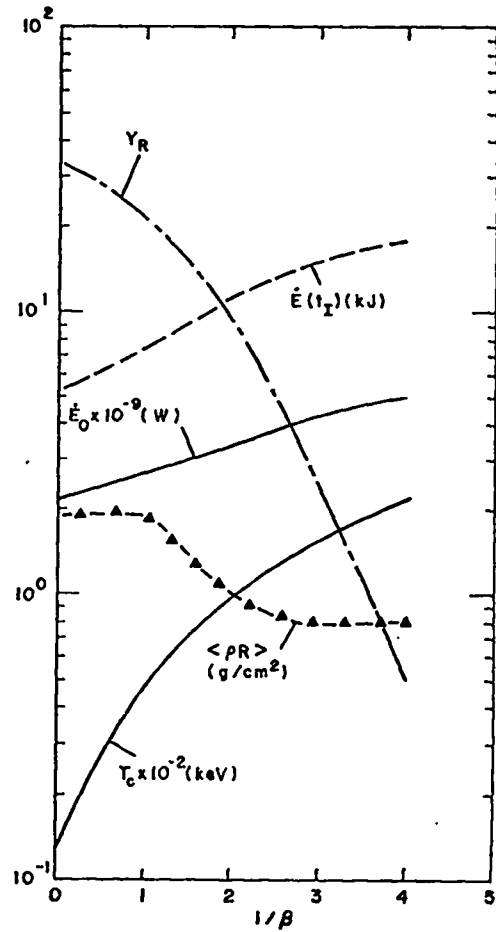
(a). The pulse exponent  $p$ ,



(b). the wavelength  $\lambda$ ,



(c). further dependents on wavelength  $\lambda$ , and



(d). the degree of flux limitation  $1/\beta$ .



$p > 1.9$ . The yield ratio passes through unity at  $p = 1.62$  and  $2.3$ . The required initial intensity  $\dot{E}_0$  declines exponentially with  $p$ . At small  $p$  excessive preheat ruins the performance; at large  $p$  the shock timing is such that a good  $\langle \rho R \rangle$  is inaccessible for  $T(0) > 8$  keV.

Performance as a function of the wavelength is described in Fig. 7(b,c). This is for the usual  $7.5\text{-}\mu\text{g}$  sphere. We give  $Y_R$ , the coronal temperature  $T_c$ , and the significant pulse parameters for both  $\beta \rightarrow \infty$  (no limiter) and  $\beta = 1$  [see (10b)]. When  $\lambda > 10.6 \mu$  we anticipate hot electron problems, when  $\lambda \lesssim 0.13 \mu$  the laser fully penetrates the uncompressed DT target. We see that with  $\beta = 1$  the largest wavelengths give the best performance. As  $\lambda$  declines and the deposition goes deeper, increased  $E(t_I)$  and  $\dot{E}(t_I)$  are needed to produce a good  $\langle \rho R \rangle$ , and still  $\langle \rho R \rangle$  at the optimal  $Y_R$  falls off. The optimal  $\dot{E}_0$  tuning for  $\beta \rightarrow 1$  is constant down to  $1.06 \mu$ , and then decreases. The difference in the yield ratio between  $\beta \rightarrow \infty$  and  $\beta = 1$  disappears below  $2 \mu$ ; the difference in the coronal temperature is gone below  $0.5 \mu$ .

Figure 7 (d) shows the optimized performance of the  $7.5\text{-}\mu\text{g}$  pellet under  $\text{CO}_2$  light as  $1/\beta = 0 \rightarrow 4$ . If the required value is  $\beta = 1$ , then the yield ratio drops from  $33.6$  to  $21.5$ ; also the required optimal energy rises from  $5.3$  to  $7.5$  kJ and  $T_c$  rises from  $13$  to  $48$  keV. If  $\beta = 0.25$ ,  $Y_R$  is down to  $0.8$ . Similar results have been obtained by Ashby and Christiansen at Culham.<sup>20</sup>

#### D. Mass Dependence

A large number of runs were made to determine the optimal pulse parameters for (1c) as a function of mass, and to examine the corresponding pellet conditions just prior to burn. The calculations were for spheres with masses ranging between  $40$  ng and  $250 \mu\text{g}$ , with the exponent  $p$  restricted to  $1.875$  and the wavelength fixed at  $\lambda = 10.6$ . We conducted a three-way optimization in  $\dot{E}_0$ ,  $\tau$ , and  $E(t_I)$ . For each time scale we found the best  $\dot{E}_0$  and  $E(t_I)$  by the procedures described in conjunction with Fig. 5(a). This was done over a range of  $\tau$  values (as for Fig. 6) until the best  $\tau$  was found. This tuning process was tedious and somewhat inaccurate, so our  $\tau$  and  $E(t_I)$  values are good to about 2%. The plotted results are principally for  $\beta \rightarrow \infty$  although

the  $Y_R$  values for  $\beta = 1$  are shown. There is little reduction in the performance at  $\beta = 1$ , especially with the larger masses. This mass dependence data is collected in Fig. 8 and Table I.

Figure 8(a) shows that  $Y_R$  exceeds breakeven at  $45$  ng; Fig. 8(b) tells us this occurs with  $60$  J of input energy. The yield ratio is  $33.6$  at  $7.5 \mu\text{g}$  and  $65$  at  $250 \mu\text{g}$  with scaling  $Y_R \sim m^{0.19}$  for  $m > 7.5\text{-}\mu\text{g}$ . The  $\langle \rho R \rangle$  of the pellet exceeds  $1$  g/cm<sup>2</sup> at  $m = 0.1 \mu\text{g}$ . It goes above  $2$  at  $m = 2 \mu\text{g}$  and above  $3$  at  $100 \mu\text{g}$ . Its scaling is  $\langle \rho R \rangle \sim m^{0.08}$  for  $m > 7.5 \mu\text{g}$  and density drops from  $1.8 \times 10^4$  g/cm<sup>3</sup> at  $70$  ng to  $1.03 \times 10^3$  g/cm<sup>3</sup> at  $250 \mu\text{g}$ . The central ion temperature at  $Y_R = 0.01$ ,  $T(0)$ , drops from  $21$  keV at  $40$  ng to  $7.5$  keV at  $0.1 \mu\text{g}$ . For larger masses  $T(0)$  is relatively constant.

The results at  $7.5 \mu\text{g}$  are essentially those of the Fig. 2 optimized implosion except that the pulse has been retuned at  $\tau = 17.1$  nsec with  $\dot{E}_0 = 1.13 \times 10^9$  W and  $E(t_I)$  is up to  $6$  kJ. The  $\langle \rho R \rangle$  of the pellet is up from  $2.09$  [Figs. 2 and 5(a)] to  $2.38$ . But the optimized yield ratio is unchanged,  $Y_R = 33.6$ .

To maintain a fixed  $\langle \rho R \rangle$  as we go to different masses the density must change in accordance with

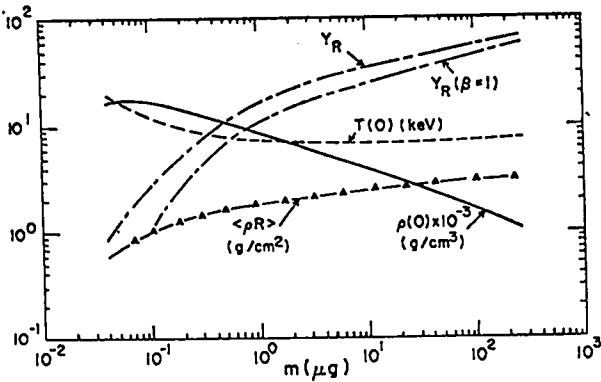
$$\rho(0) \sim \langle \rho R \rangle^{3/2} / m^{1/2} . \quad (14)$$

Generally, it is desirable to have  $\langle \rho R \rangle \gtrsim 2$  for efficient propagating burn, or at least  $\langle \rho R \rangle \gtrsim 1$  for bootstrap-heating.

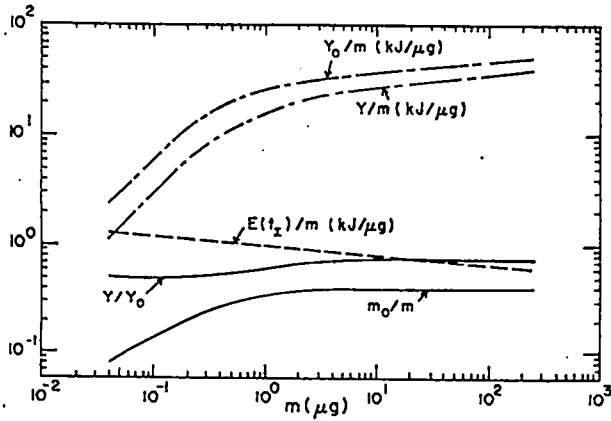
As we go to small masses, however, the density must be made so large for  $\langle \rho R \rangle \gtrsim 1$  or  $2$  that (a) the  $\alpha$ -particle mean free path becomes too long for effective bootstrap-heating [see Ref. 7, Fig. 1(a)], and (b) the large internal energy of degeneracy neutralized the yield multiplication from propagating burn. Thus, the  $40\text{-ng}$  pellet is optimized when  $\langle \rho R \rangle = 0.6$  and  $\rho(0) = 1.6 \times 10^4$  g/cm<sup>3</sup>. Achievement of  $\langle \rho R \rangle = 2$  would require further compression to  $\rho(0) = 8 \times 10^4$  g/cm<sup>3</sup>. The optimized tuning in  $\dot{E}_0$  sets  $T(0)$  at  $21$  keV, which is the best temperature for burn in the absence of bootstrap-heating and propagation.

With larger masses it is easier to get a good  $\langle \rho R \rangle$ , but excessive input energy may be required.

Fig. 8. Mass dependence of



(a). optimized pellet performance characteristics,



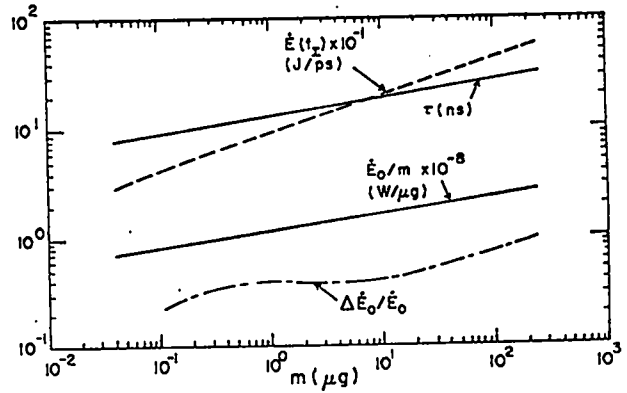
(b). further optimized pellet performance characteristics,

At 250  $\mu\text{g}$ ,  $\langle \rho R \rangle = 3.1$  with only  $\rho(0) = 1.03 \times 10^3$   $\text{g/cm}^3$ , but 150 kJ must be supplied. In any case, the optimally imploded pellets manifest only a gradual  $\langle \rho R \rangle$  increase with mass, since beyond  $\langle \rho R \rangle \approx 2.5$  fuel depletion severely limits any additional yield from greater inertial confinement.

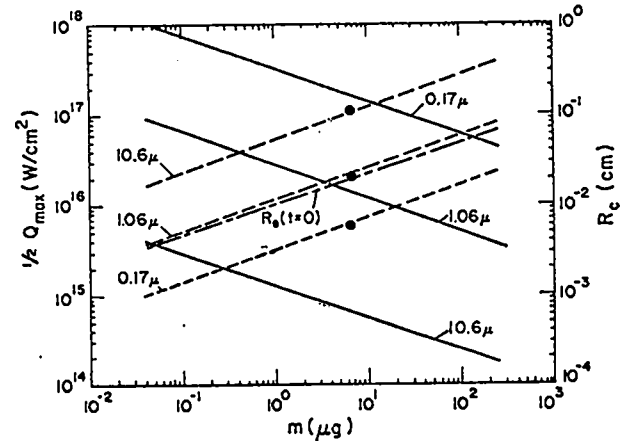
As an estimate of the core mass we use

$$m_0 = \frac{4\pi}{3} \frac{\langle \rho R \rangle^3}{\rho^2(0)} \quad (\mu\text{g}) \quad (15)$$

with  $\langle \rho R \rangle$  and  $\rho(0)$  obtained from the Fig. 8(a) data. The resultant  $m_0/m$  ratio is plotted in Fig. 8(b). It levels off at  $m_0/m = 0.40$  for  $m > 7.5 \mu\text{g}$ . Thus,



(c). the optimal pulse parameters, and



(d). the half-intensity  $1/2 Q_{\text{max}}$  at peak power, the critical radius  $R_c$  at various wavelengths, and initial radius of the pellet edge  $R_e(t=0)$ .

the core constitutes 40% of the mass in larger, optimally imploded pellets.

The yield from uniformly heated cores is

$$Y_0 = 326 \frac{m_0 \langle \rho R \rangle}{(6.3 + \langle \rho R \rangle)} \text{ (kJ)} \begin{cases} \langle \rho R \rangle > 1 \\ T(\text{burn}) > 20 \text{ keV,} \end{cases} \quad (16)$$

based on (5d and e). We have plotted  $Y_0/m$  in Fig. 8(b). Also we give  $Y/m = Y_R \times E(t_x)/m$  from the full implosion simulations, as well as the ratio  $Y/Y_0$ . Clearly,  $Y/Y_0$  levels off at 0.75. So with optimization, central ignition and propagating burn extract  $\sim 75\%$  of the yield available from uniformly heated cores.

Above 7.5  $\mu\text{g}$  the optimized yield scales as  $Y \sim m^{1.12}$ . The requisite energy runs from 1.23 kJ/ $\mu\text{g}$  at 40 ng, where the influence of degeneracy is most severe, down to 0.65 kJ/ $\mu\text{g}$  at 250  $\mu\text{g}$  where propagating burn is most effective. The energy scaling is  $E(t_I) \sim m^{0.93}$ . Together, these results scale the yield ratio as  $Y_R \equiv Y/E(t_I) \sim m^{0.19}$ .

Alternatively,  $Y_R \sim \varepsilon G_O M_C^n$  from (9), assuming  $M_n$  and  $M_I$  are constant. Above 7.5  $\mu\text{g}$  at optimum,  $I_O$  is constant (at its  $\sim 7.5$ -keV value) and  $m/m_O = 0.40$ , while  $Y/Y_O = 0.75$ . Thus,  $G_O \equiv Y_O/m_O I_O \sim Y_O/m_O \sim Y/m \sim m^{0.12}$ . Consequently, the product  $\varepsilon M_C^n \sim m^{0.07}$ , and  $M_C \equiv (Y/Y_O)/(I/I_O) \sim I^{-1}$ . Now, if we had pure adiabatic compression of the core, from constant initial conditions up to  $\rho(0)$ , then  $I \sim \rho(0)^{2/3} \sim (m^{-.41})^{2/3} \sim m^{-.27}$  [from the Fig. 8(a) data]. Thus, for a constant coupling coefficient  $\varepsilon$  this would say that  $\varepsilon M_C^n \sim m^{-.27}$ , which is too large by a factor  $m^{-.20}$ . The discrepancy is explained by the fact that for optimal tuning the first shock crossing the core must be progressively stronger, as the mass increases. This is demonstrated below. Thus, the initial core temperature prior to adiabatic compression is correspondingly higher--raising the requirements on  $I$  and  $E(t_I)$ .

Figure 8(c) shows that the optimal time scale runs from  $\tau = 8$  nsec when  $m = 40$  ng to  $\tau = 30$  nsec when  $m = 250$   $\mu\text{g}$ . Thus, for reasons still unclear  $\tau \sim m^{1/6} \sim R_e^{1/2}$  ( $t = 0$ ). Pellet performance drops rapidly if  $\tau$  is too short, as evident from the Fig. 6 results. We find that a 12.5-nsec time scale is sufficient for good performance over the whole mass range investigated, but at 250  $\mu\text{g}$ , for example,  $Y_R$  drops from 65 to 38 for a reduction  $\tau = 30 \rightarrow 12.5$  nsec.

We find that the optimal initial pulse power obeys the scaling rule

$$\dot{E}_O \sim m^q \quad (17)$$

with  $q = 1.15$ . Our earlier Ref. 3 found that  $q = 1.5$  with  $p = 2$  and  $\tau$  fixed at 20 nsec. A rough justification of (17) follows from assuming that the optimal initial power launches a first shock obeying  $\dot{E}_O \sim P v_s R^2(t=0)$ . The shock speed  $v_s$  and fluid velocity  $v_o$  vary as  $v_s \sim v_o \sim (P/\rho_o)^{1/2}$  with  $\rho_o$

the density of solid DT - a constant, so  $P \sim v_o^2$  and  $\dot{E}_O \sim v_o^3 R^2$ . With proper timing  $v_o \sim R/\tau$  and  $R \sim m^{1/3}$ , while  $\tau \sim m^{1/6}$ . Thus, finally,  $\dot{E}_O \sim R^5/\tau^3 \sim m^{5/3}/m^{1/2} \sim m^{1.15}$ , as observed. This emphasizes that the optimal tuning for all masses gets the first shock to the origin at  $t = \tau$ . Also, we see that the first shocks are stronger for larger masses, being launched by an increasing pressure  $P_O \sim \rho_o v_o^2 \sim R^2/\tau^2 \sim m^{0.33}$ .

The  $\Delta \dot{E}_O/\dot{E}_O$  curve in Fig. 8(c) gives the range of  $\dot{E}_O$  values about the optimum over which  $Y_R > 1$  is obtained for each mass. Clearly, the tuning requirements become less stringent at higher masses, so that with a 250- $\mu\text{g}$  sphere, more than 100% deviation in  $\dot{E}_O$  is permissible. The permissible error with spheres as targets is significantly greater at low masses than with the shells discussed in Ref. 3. With a 2.7- $\mu\text{g}$  sphere (absorbing 2.4 kJ) more than a 40% deviation in  $\dot{E}_O$  is allowed as compared to a permissible 3% error in the Ref. 3 shell of the same mass.

The peak input power for the optimized implosions varies as  $\dot{E}(t_I) \sim m^{0.34}$  as required by (3) when  $\tau \sim m^{1/6}$ . Thus, the final power runs from 29 J/psec at 40 ng to 550 J/psec when  $m = 250$   $\mu\text{g}$ .

Figure 8(d) plots half the peak intensity required for the optimized  $\text{CO}_2$  implosions at the various masses, and gives the calculated  $\text{CO}_2$  critical radii at peak power;  $1/2 Q_{\text{max}} = \dot{E}(t_I)/8\pi R_c^2$ . The half-intensity is recorded, since in a classical calculation of the thermal transport, only half of terminal energy input flows from the critical surface toward the core.

We see that at 250  $\mu\text{g}$  the  $\text{CO}_2$  critical surface has expanded to 0.37 cm, so that the absorptive surface area exceeds 1  $\text{cm}^2$ . We observe no significant readjustment in the location of  $R_c$  with changes in  $\tau$  from 30 nsec to 12.5 nsec and pulse reoptimization.

The critical radii for 1.06  $\mu$  and 0.17  $\mu$  were derived by noting that in optimally imploded pellets the density falls as  $R^{-3}$ , largely independent of the deposition wavelength. Thus, we used, for example,

TABLE I (b)

$$\frac{R_c(1.06)}{R_c(10.6)} = \left( \frac{\rho_c(10.6)}{\rho_c(1.06)} \right)^{1/3} = \left( \frac{1.06}{10.6} \right)^{2/3} =$$

1/4.64,

and similarly,  $R_c(0.17)/R(10.6) = 1/15.7$ . The derived radii are slightly above the radii calculated (denoted by  $\bullet$ ) in the optimized performance vs wavelength simulations for Fig. 7 (b and c), which provide a cross-check on the procedure. The half-intensities at 1.06  $\mu$  and 0.17  $\mu$  were obtained by using the  $\text{CO}_2$  peak powers and the derived critical radii. Since Fig. 7(c) showed that the peak power requirements rise above the  $\text{CO}_2$  values as we go to shorter wavelength, the precise derived half-intensities should be somewhat higher than indicated.

On Figure 8(d) we have included the initial pellet edge radius  $R_e(t=0)$  vs its mass. It is interesting to note that at peak power the 10.6- $\mu$  critical surface has moved out considerably from its initial position [i.e., from  $R_c(t=0)$ ], the 1.06- $\mu$  surface is essentially unmoved, and the 0.17- $\mu$  critical radius has descended to one-third its initial value.

Examination of the Table I(b) entries shows that for lower peak intensities,  $\dot{E}(t_1)/4\pi R_c^2$ , and the resultant favorable reduction in hot electron production, it is desirable to go to the most massive pellet feasible under the energy constraints of the available laser system.

TABLE I. Optimized pellet performance characteristics vs mass;  $p = 1.875$ .

TABLE I (a)

$m$ ( $\mu\text{g}$ )	$Y_R$	$Y_R(\beta=1)$	$\rho(0)$ $\text{g}/\text{cm}^3$	$\langle \rho R \rangle$ $\text{g}/\text{cm}^2$	$T(0)$ keV	$R_c(t=0)$
0.04	0.9	--	$1.60 \times 10^4$	0.58	19.5	35
0.11	3.0	1.2	$1.7 \times 10^4$	1.03	11.9	50
0.27	7.2	3.8	$1.31 \times 10^4$	1.35	8.6	67
0.70	13.3	8.7	$9.5 \times 10^3$	1.75	7.5	92
7.50	33.6	22.0	$4.3 \times 10^3$	2.33	6.6	203
22.0	39.0	29.0	$3.0 \times 10^3$	2.65	6.9	291
58.0	49.0	38.0	$2.1 \times 10^3$	2.94	7.3	402
250.0	65.0	55.0	$1.03 \times 10^3$	3.10	7.4	654

$m(\mu\text{g})$	$\dot{E}(t_1)$ kJ	$t_1(\text{nsec})$	$\dot{E}_0$ (W)	$\Delta \dot{E}_0 / \dot{E}_0$	$\dot{E}(t_1)$ (J/psac)	$R_c(10.6)\mu$	$R_c(1.06)\mu$
0.04	.05	8.0	$2.7 \times 10^6$	---	29	167	37
0.11	.129	9.3	$9.5 \times 10^6$	.23	42	240	54
0.27	.292	10.7	$2.6 \times 10^7$	.34	59	320	73
0.70	.700	12.3	$7.3 \times 10^7$	.38	82	460	101
7.5	6.	17.	$1.2 \times 10^8$	.38	175	1080	230
22.	15.8	21.	$4.0 \times 10^8$	.47	250	1570	340
58.	41.	24.	$1.23 \times 10^9$	.62	345	2700	480
250.	155	30.	$6.4 \times 10^{10}$	.95	560	3700	800

## IV. CONCLUSION

We have given detailed results from computer calculations of the hydrodynamics and burn of optimally imploded DT spheres. We have shown how conditions in the pellet core prior to burn are affected by variations in the pulse shape parameters. Burn performance was related to these pellet conditions with the aid of our earlier burn study results. For yields exceeding breakeven considerable precision in the pulse shape is demanded. Degraded performance is anticipated from the presence of hyperthermal electrons generated at the high peak laser power levels required for optimized sphere implosions. Both the hyperthermal production and the precision needs can be reduced by going to larger pellets and correspondingly higher input energies.

## REFERENCES

1. S. Neddermeyer, as described in D. Hawkins, LASL report No. LAMS-2532, 1961 (unpublished), Vol. I, p. 23.
2. J. Nuckolls, T. Wood, A. Thiessen, and G. Zimmerman, Nature (London) 239, 139 (1972).
3. J. S. Clarke, H. N. Fisher, and R. J. Mason, Phys. Rev. Lett. 30, 89(1973), and Phys. Rev. Lett. 30, 249 (1973).
4. K. Brueckner, IEEE Transactions on Plasma Sciences PS-1, 13 (1973).
5. K. Boyer, Bull. Am. Phys. Soc. 17, 1019 (1972), and Aeronautics and Astronautics 11(1), 28(1973).
6. J. Nuckolls, J. Emmett and L. Wood, Physics Today, August (1973).
7. G. S. Fraley, E. J. Linnebur, R. J. Mason and R. L. Morse, Phys. Fluids 17, 474(1974).
8. D. Forslund, J. Kindel and E. Lindman, Phys. Rev. Lett. 30, 739 (1973).

9. L. Spitzer, Physics of Fully Ionized Gases (Interscience, New York, 1969) Chap. V.
10. J. L. Tuck, Nucl. Fusion 1, 202 (1961).
11. H. Brysk, P. M. Cambell, and P. Hammerling, KMS Fusion Report No. V110 (1973).
12. R. Courant and K. O. Friedrichs, Pure and Applied Mathematics Vol. I, Supersonic Flow and Shock Waves (Interscience, New York 1948), Chap. III E.
13. C. Fauquignon and F. Floux, Phys. Fluids 13, 386 (1970).
14. J. L. Bobin, Phys. Fluids 14, 2341 (1971).
15. R. L. Morse and C. W. Nielson, Phys. Fluids 16, 909 (1973).
16. D.W. Forslund, J. Geophys. Res 75, 17 (1970).
17. T. M. O'Neil and M. N. Rosenbluth, IDA Report No. P-893 (1972).
18. R. E. Kidder and J. W. Zink, Nucl. Fus. 12, 325 (1972).
19. K. Lee, D. B. Henderson, W. P. Gula, and R. L. Morse, Bull. Am. Phys. Soc. 18, 1341 (1973).
20. J. P. Christiansen, and D. E. Ashby, Sixth European Conference on Controlled Fusion and Plasma Physics, Moscow, USSR. 30 July - 3 August 1973.
21. P.A.G. Scheuer, Monthly Notices Roy. Astron. Soc. 120, 231 (1960).

#### APPENDIX

We calculate the inverse-bremsstrahlung energy absorption, using Scheuer's<sup>21</sup> free-free coefficient

$$K_a = \frac{8\pi}{3} \frac{e^6 Z^3 \lambda^2 n^2}{c^3 (2\pi m_e k T_e)^{3/2}} (1 - n/n_c)^{-1/2} (\ln \Lambda' - 5\gamma) \quad (\text{A-1})$$

in which the critical density is  $n_c = \frac{\pi m_e c^2}{e^2 \lambda^2}$ ,  $\Lambda' = (8k^3 T_e^3 \lambda^2) / \pi^2 m_e c^2 e^4 Z^2$ , and  $\gamma$  is Euler's constant, 0.577...

Electrons in the computational zones of width  $\Delta m$  acquire specific energy via inverse-bremsstrahlung at a rate

$$\dot{S}_{e_i} = (1 - e^{-K_a \Delta R}) e^{-\sum K_a \Delta R} \dot{E}(t) / \Delta m. \quad (\text{A-2a})$$

Here the sum,  $\sum K_a \Delta R$ , is taken from the pellet edge to the zone just before the critical density, and  $\dot{E}(t)$  is the laser power (1c). The calculations assume total anomalous absorption of all of the remaining energy by dumping it into the thermal electrons in the first cell where  $n$  exceeds  $n_c$ . Per unit time and mass this is

$$\dot{S}_{e_a} = e^{-\sum K_a \Delta R} \dot{E}(t) / \Delta m. \quad (\text{A-2b})$$

These two rates plus the specific burn energy redeposition rate constitute the  $\dot{S}_e$  source term in Eq. (b-2a) of Ref. 7.

Tapered zoning was employed to improve the resolution and efficiency of the calculations. Thus, initially, the zoning was finer at the pellet center and edge, than in its midregions. At the center  $\Delta R/R_e(t=0) = 5 \times 10^{-3}$ . The neighboring zones increase in size by the ratio  $\Delta R_{m+1} / \Delta R_m = 1.2$ . At the edge  $\Delta R/R_e(t=0) = 1.3 \times 10^{-3}$ , while the lower zones are larger by  $\Delta R_{m-1} / \Delta R_m = 1.053$ . This generates 81 zones in total. For the 7.5- $\mu$ g pellet,  $R_e(t=0) = 203 \mu$ , the starting zone widths were 1.01  $\mu$  at the center, 0.28  $\mu$  at the edge, and the 11th zone from the center was the largest-- 7.4  $\mu$ .